ADVANCED HEALTHCARE MATERIALS
www.advhealthmat.de

3D Cell Migration Chip (3DCM-Chip): A New Tool toward the Modeling of 3D Cellular Complex Systems

*Silvia Buonvino, Davide Di Giuseppe, Joanna Filippi, Eugenio Martinelli, Dror Seliktar, and Sonia Melino**

3D hydrogel-based cell cultures provide models for studying cell behavior and can efficiently replicate the physiologic environment. Hydrogels can be tailored to mimic mechanical and biochemical properties of specific tissues and allow to produce gel-in-gel models. In this system, microspheres encapsulating cells are embedded in an outer hydrogel matrix, where cells are able to migrate. To enhance the efficiency of such studies, a lab-on-a-chip named 3D cell migration-chip (3DCM-chip) is designed, which offers substantial advantages over traditional methods. 3DCM-chip facilitates the analysis of biochemical and physical stimuli effects on cell migration/invasion in different cell types, including stem, normal, and tumor cells. 3DCM-chip provides a smart platform for developing more complex cell co-cultures systems. Herein the impact of human fibroblasts on MDA-MB 231 breast cancer cells' invasiveness is investigated. Moreover, how the presence of different cellular lines, including mesenchymal stem cells, normal human dermal fibroblasts, and human umbilical vein endothelial cells, affects the invasive behavior of cancer cells is investigated using 3DCM-chip. Therefore, predictive tumoroid models with a more complex network of interactions between cells and microenvironment are here produced. 3DCM-chip moves closer to the creation of in vitro systems that can potentially replicate key aspects of the physiological tumor microenvironment.

1. Introduction

Cellular in vitro models of tissues and organs are simplified surrogates with respect to real human tissues, which have yet limited use in clinical diagnosis and drug development due to their high costs and fail to provide a comprehensive and predictive screening platform comparable to the genetic variability of the in vivo systems.[1–4] Another relevant problem related to in vitro systems is the reproducibility of the microenvironment of cell niches.[5] Therefore, the optimization of 3D cell culture systems which, compared to 2D cultures, more closely mimic the in vivo conditions, is of crucial importance in cell biology and for pharmaceutical approaches. Recent technological advances in materials design and 3D cell culture systems have led to the control of complex cellular interactions, such as cell-cell and cell- biomaterial.[6–11] Thanks to gelling processes compatible with cell survival, it is now possible to create scaffolds that mimic the extracellular matrix (ECM) and the 3D physiological environment, providing the optimal conditions for the creation of 3D growth systems of both stem and tumor cells. A relevant study target in cancer- and stem cell-based systems is cell migration or invasiveness. In general, cell migration is stimulated and directed by the interaction of cells with the ECM, neighboring cells, or chemotactic and physical agents. For instance, cell migration has crucial relevance in almost all morphogenic processes during embryogenesis, ranging from gastrulation to neural development. Moreover, in the adult organism, cell migration contributes to physiological and pathological conditions and it is essential for the development of therapies that influence wound healing, inflammation, and tumor metastases.[12] Finally, the mechanisms of migration can be understood by analyzing the response to modulator molecules (inhibitors or activators) of cell migration. Cell migration is a cyclic process, in which a cell extends its protrusions in its front, it is stabilized by the formation of adhesive complexes and then retracts at the rear end, allowing the cell to advance onto its substrate. Therefore, the integration of signaling events and changes in cellular architecture are required, and both, the cell-substrate adhesiveness and the 3D cell environment play a significant role in determining the migration type and rate.[13,14]

S. Buonvino
Department of Experimental Medicine
University of Rome Tor Vergata
Rome 00133, Italy

D. Di Giuseppe, J. Filippi, E. Martinelli
Department of Electronic Engineering
University of Rome Tor Vergata
Rome 00133, Italy

D. Seliktar
Department of Biomedical Engineering
Technion Israel Institute of Technology
Haifa 3200003, Israel

S. Melino
Department of Chemical Science and Technologies
University of Rome Tor Vergata
via della Ricerca Scientifica, Rome 00133, Italy
E-mail: sonia.melino@uniroma2.it

S. Melino
NAST Center- University of Rome Tor Vergata
via della ricerca scientifica, Rome 00133, Italy

The ORCID identification number(s) for the author(s) of this article can be found under https://doi.org/10.1002/adhm.202400040

DOI: 10.1002/adhm.202400040

Consequently, the synthesis and optimization of biomaterials and the fabrication of new devices for quantifying and visualizing cell migration/invasion have become central to research in the life sciences. In vitro models that evaluate the efficacy of potential new drugs must be designed for specific cell behaviors. Several methods have been developed to study cell motility from the wound healing test with scratching into a 2D cell monolayer,[15,16] to the Boyden chamber test, also known as the trans-well migration assay,[17] and to new generation devices, named lab-on-a-chip.[18–26] However, some of these methods do not allow to have a good 3D system, a specific control on the substrate surface chemistry, and/or a correct mimic of the cellular microenvironment. Recently, a 3D gel-in-gel system, based on a polyethyleneglycol-fibrinogen instead of PEG-fibrinogen (PEGDA-fibrinogen) hydrogel (PFHy), was developed by Ivanir et al. using fibroblasts and tumor cells to evaluate their invasive power.[27] The study of cell migration in the 3D gel-in-gel system consists of a hydrogel sphere (inner gel) containing cells at a well-defined cell density, which is embedded into an external gel (outer gel) with a lower Young's modulus, in order to promote the migration of cells from the sphere. The outer gel may also contain biochemical factors or drugs whose effects on cell migration are to be studied. PFHy was widely used for several cell lines[28–32] and it has been used for the easy production of tunable microspheres with control over rheology and cell density.

Microspheres of cells are produced by embedding cells in PFHy by cross-link formation of a precursor solution following a radical photopolymerization reaction.[28,33] Subsequently, the gel spheres are placed in the precursor solution of the outer gel, and the polymerization of the latter is carried out inside the multi-well. The chemical composition and biological nature of the two gels, as well as their relative positioning, provide a framework for creating intricate spatiotemporal scenarios with living cells in situ. The driving force of the system is the innate motility of the cells which leads them to invade the external gel at different speeds and with different motility mechanisms.[27] It is the modulation of the properties of the external hydrogel and the consequences on cell motility that provide a quantitative response to potential therapeutic treatments.

Here we have optimized this gel-in-gel assay, improving its feasibility. A lab-on-a-chip, named 3DCM-chip,[34] was designed and optimized using a microfluidic system, offering many advantages compared to the traditional methods. Several analyses were here performed in order to demonstrate that 3DCM-chip provides a smart platform to analyze the effects of chemico-physical stimuli on migration/invasion of different cell types, such as mesenchymal stem cells, fibroblasts, and tumour cells, and to allow easier development of more complex co-culture systems. Cellular invasion of triple-negative breast cancer cells of the MDA-MB 231 cellular line was here studied, analyzing the effects of the presence of other cellular lines using co-cultures with normal human dermal fibroblasts (NHDFs), mesenchymal stem cells (MSCs) and human umbilical vein endothelial cells (HUVECs), in order to create predictive tumoroids models taking into account the network of interactions between cancer cells and tumor microenvironment (TME), which is an indispensable element for a deep and complete understanding of the tumor disease. The ease of use of our device can also suggest its possible application to develop new antitumor therapeutic approaches, such as cell- and physical-therapy.

2. Results and Discussion

2.1. 3D Cell Migration Chip: A New Tool to Study 3D Cell Migration; Design and Production of 3DCM-Chip

The development of the 3DCM-chip[34] is based on the experience gained from small-scale gel-in-gel assays.[27] This microfluidic device is designed to simplify and enhance the reproducibility of the gel-in-gel system's preparation. It also allows for the use of smaller quantities of cells and expensive reagents, reducing resource requirements. 3DCM-chip consists of a poly-styrene base at the bottom and upper layers made from extruded and cast poly(methyl methacrylate) (PMMA). PMMA is a biocompatible material that provides excellent transparency for microscopic analysis of samples and effectively prevents the permeation of small molecules. In **Figure** 1A–C the schematic representation of the components of the chip and the digital images of the implemented system are shown.

To facilitate the in situ polymerization of cell spheres, the precursor gel solution can be dropped onto a removable super-hydrophobic surface at the bottom of the well. This removable super-hydrophobic surface can take various forms and exhibit different levels of hydrophobicity, depending on the type of polymer used. For instance, it may consist of a nano-structured plastic polymer like polydimethylsiloxane (PDMS) and,[35] when using hydrophilic gel precursor solutions, such as (PEG-protein hydrogels, this ensures a perfectly spherical deposition of the solution, which can then be polymerized using UV photo-polymerization. The chip allows for the easy generation of inner gel spheres (0.4–2 mm in diameter) with volumes ranging from 1 to 5 µL using micro-pipettes (Figure 1D). Depending on the desired size of the spheres, external gels can be produced with volumes between 50 and 100 µL. Furthermore, the 3DCM-chip supports the creation of gel-in-gel structures using various types of both thermal and photo-polymerizable polymers, including agarose, gelatin, and PEG-based hydrogels. This versatility makes it a valuable tool for conducting controlled experiments in the context of 3D cell migration studies and other related research.

The 3DCM-chip represents a significant advancement in the field, as it greatly facilitates and enhances the preparation of the system, making it highly reproducible for operators. It allows for the use of smaller quantities of cells and reagents, which are often expensive. Additionally, it incorporates a removable superhydrophobic nanostructured surface to optimize the in situ production of cellular microspheres. One particularly critical aspect of the process, in fact, involves creating the microspheres on plates with functionalized surfaces (e.g., Aerosil). These spheres must be then transferred to multi-plates or dishes where the outer gel is polymerized. This represents a crucial step with the possibility of damaging or fragmenting the spheres, resulting in sample loss. The 3DCM-chip streamlines these operations, making them more manageable and significantly reducing the risk of sample damage. This not only improves the quality and integrity of the samples but also optimizes costs, analysis times, and the overall

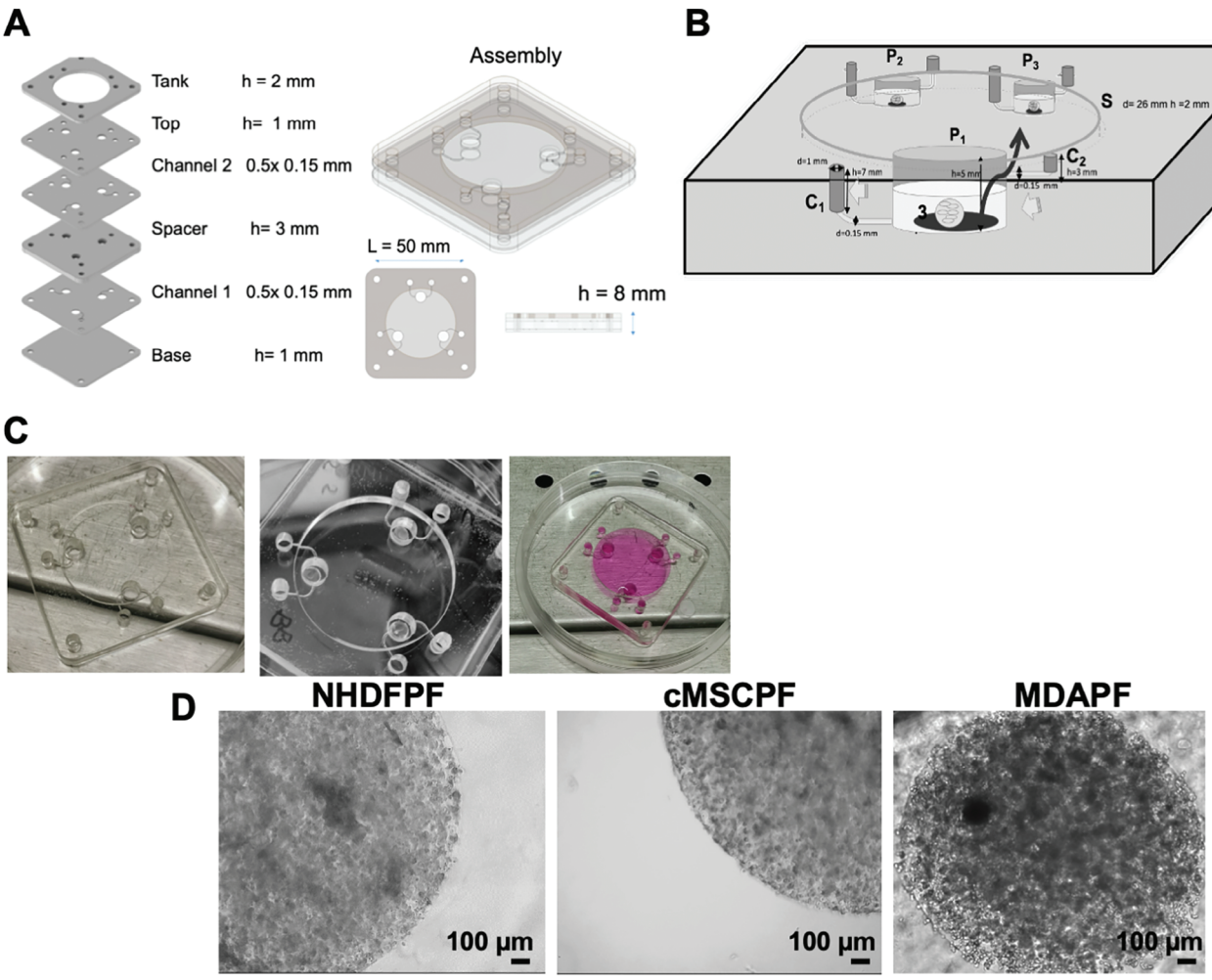

Figure 1. Design and production of the 3DCM-chip. A) CAD drawing and sliced view of the 3DCM-chip; B) schematic representation of the chip constituted by: an inner well containing the gel-in-gel system (P d = 5 mm vol. 98 µL h = 5 mm), an outer well (vol. 60 µL) containing the culture medium (S vol. 1.2 mL), the bottom-channel (1 0.5 × 0.15 mm) for washing the cell microsphere (inner gel with cells 1–5 µL) previously produced in situ on a removable super-hydrophobic surface ( ) (3), and the upper channel (2 0.5 × 0.15 mm) for removing the medium once the gel-in-gel system is prepared; C) digital photographs of the 3DCM-chip; D) brightfield micrographs of the gel-in-gel systems with cell spheres NHDFPF, cMSCPF and MDAPF. Scale bars are of 100 µm.

experimental reproducibility, making it a valuable tool for researchers in various fields.

The validation of the chip for testing cell migration in the gel-in-gel system (**Figure 2**A) was carried out with different cell types, including human cardiac mesenchymal stem cells (cMSCPF), normal human dermal fibroblasts (NHDFPF) and MDA-MB 231 breast cancer cells (MDAPF), as shown in Figure 2B. Interestingly, under the same experimental conditions, these types of cell lines exhibited different behaviors.

Specifically, MDAPF demonstrated pronounced cell invasion into the outer gel, while NHDFPF showed a less invasion ability. NHDFPF showed less invasion compared to breast cancer cells. The protrusions length after day 6 of culture was 154.8 ± 42.4 µm calculated by ImageJ software (collecting 12 measurements for each biological replica). The quantitative analysis of the cell migration can be performed by measuring the size of the circular crown around the cell sphere using the following equation:[27]

$$\text{migration index} = \frac{\pi * \left(R^2_{\text{average}} - r^2_{\text{average}} \right)^{\text{sample}}}{\pi * \left(R^2_{\text{average}} - r^2_{\text{average}} \right)^{\text{control}}} \quad (1)$$

where R is the average of final radius and r is the average of radius at time 0. Using this analysis, the migration index of cells of NHDFPF spheres compared to the MDAPF migration (as control) was 0.4967 ± 0.0752 (± S.D.).

Notably, cMSCPF after 5 days of growth did not exhibit any invasion into the outer gel (Figure 2B). This observation highlights the distinct migratory capabilities of these different types

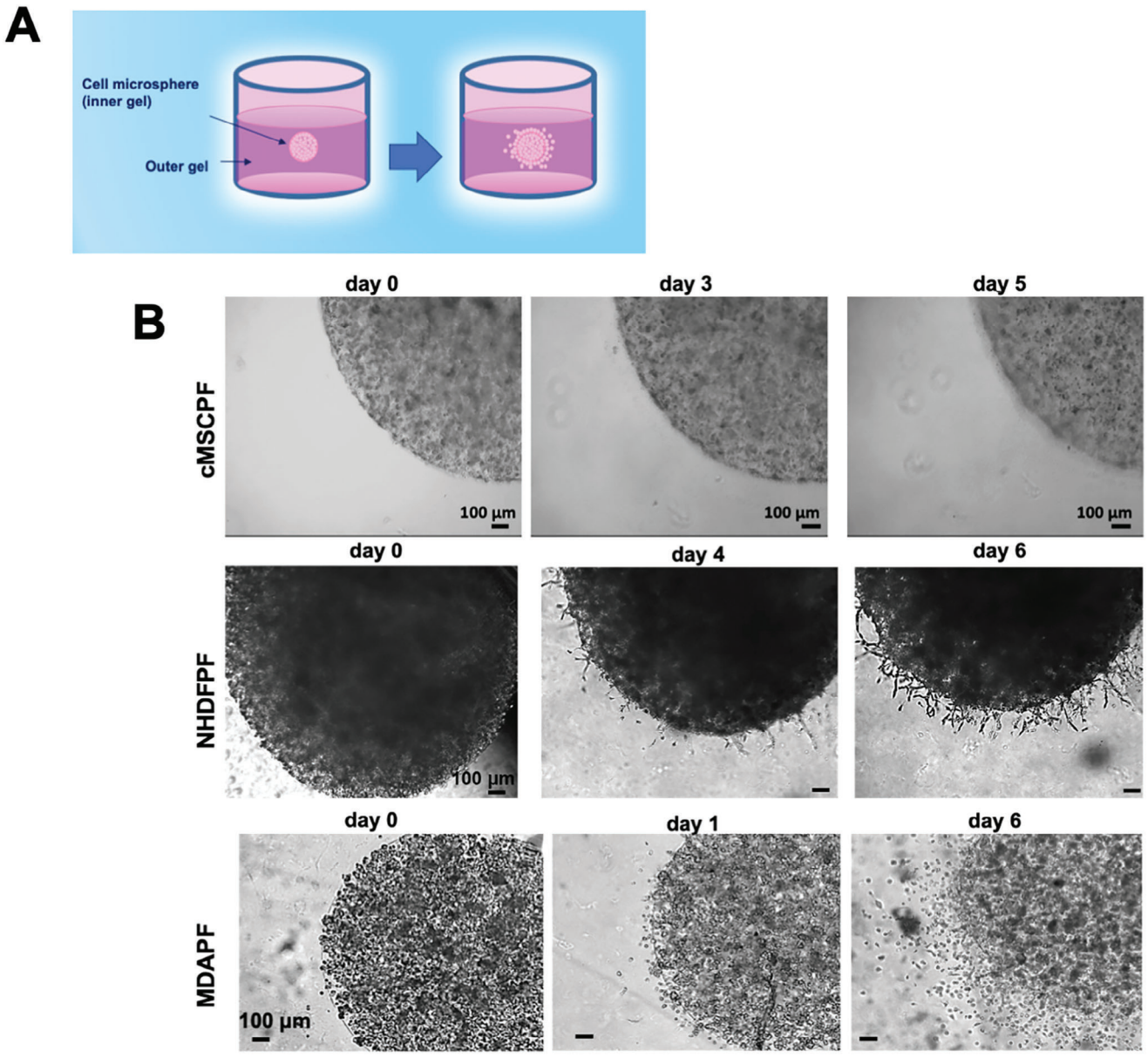

Figure 2. 3DCM-chip for assessing the invasion of different cell types in the gel-in-gel system. A) Schematic representation of the gel-in-gel system; B) brightfield micrographs of PFHy cell microspheres cMSCPF, NHDFPF and MDAPF and their invasion in the outer gel over time. Experiments were performed in four biological replicates. Scale bars are of 100 µm.

of cell lines in the 3DCM-chip system. The differences in the behavior are linked to specific protein expression patterns unique to each of the examined cell lines. The implementation and optimization of this system could in the next future lead also to the production of an in vitro organotypic model of the stem niches, where adult stem cells (ASC) are found. In fact, it is reported that ASCs are present in specific niches with a biochemically controlled microenvironment, which have the function of maintaining cell plasticity in adult life and to limit the processes of differentiation.[36] In these niches, whose presence has been found in numerous tissues and organs of the adult individual,[37] such as the endothelium, skeletal and cardiac muscle, liver, and cornea, the ASCs remain confined and relatively quiescent until reactivated by damages or diseases.

Therefore, the mimesis of these niches in the 3DCM-chip may be optimal for studying the biochemical mechanisms responsible for stem cell migration and reactivation in tissue repair and regeneration.

Currently, tumor-on-a-chip are promising platforms to facilitate the development of cancer therapies and,[38] in this context, the 3DCM-chip can be used as a tool for the analysis of the action of potential inhibitory or stimulatory drugs on cancer cell invasiveness. Moreover, 3DCM-chip could be used with different types of spheroids obtained with or without hydrogels.

Preliminary gel-in-gel assays have been also performed using spheroids without hydrogel, directly obtained in the 3DCM-chip (data not shown). Experimental studies are also in progress with other photopolymerizable hydrogels in order to have a wider diffusion of our device.

Given the importance of the physiological role of hydrogen sulfide (H_2S), in recent years, many studies have been focused on exploring the potential use of exogenous H_2S donors for treating diseases associated with both reduced endogenous H_2S levels and the activation of oxidative and pro-inflammatory processes. Slow-releasing H_2S donors have displayed significant therapeutic potential, and some are currently undergoing clinical investigation for the treatment of cardiovascular,[39,40] neurodegenerative,[41,42] and gastrointestinal pathologies,[43,44] and of cancer.[45–48] H_2S-releasing donors have also been shown to reduce the viability and migration of breast cancer cells in 2D cell cultures.[48–52] In our recent studies the cell invasiveness of tumoroid of the MDA-MB 231 breast cancer cell line has been also studied using the gel-in-gel assay and the 3DCM-chip (here described in detail).[53] We observed an increased cell invasiveness in the presence, in the cell culture medium, of a glutathionylated garlic extract (GSGa), which is a slow-releasing H_2S-donor,[28,49,54,55] at a concentration releasing 17.0 μM of H_2S and an inhibition only at higher concentration (34.0 μM of H_2S). Although the molecular mechanism is not completely known, the up-regulation of the cyclin D1 and the increase of the activation of ERK1/2 were observed after treatment at low concentration of H_2S-donor in the 3D cellular models.[53] These results showed the great potential of the 3DCM-chip as a platform for drug testing in more in vivo-like cellular models.

2.2. Toward the Mimesis of TME: Cell Co-Culture Systems in the 3DCM-Chip

2.2.1. 3DCM-Chip of Co-Cultures for Monitoring the Effects of Diffusible Biochemical Stimuli

In our quest to enhance the reliability of our 3D hydrogel-based tumoroid models, we harnessed the advantages provided by the 3DCM-chip. This innovative platform enabled us to create more sophisticated cell co-culture systems with the capacity to better mimic the intricate features of the physiological TME. 3D co-culture systems in PFHy were used to investigate the impact of fibroblasts, which are essential components of the TME, on the invasiveness of breast cancer cells of the MDA-MB 231 cell line.

Different experimental setups were used in order to analyze the effects on the cancer cell invasion due to diffusible biochemical factors. First, we analyzed the compartmentalization of the cells reducing the physical interactions between the different cell types. MDAPF sphere was cultured into an outer gel in which was present an NHDFPF or an MDAPF sphere (**Figure 3A**). In this scenario, MDA-MB 231 cell migration was assessed.

The cell invasion after one and 6 days of culture was evaluated (Figure 3B) and an increased migration of cells in the MDAPF sphere was observed only in the case of the presence of two MDAPF spheres, on the contrary, any increase was observed in the presence of the NDHFPF sphere at the investigated times.

Consistently, the same experiment was performed by culturing a mCherry/MDAPF sphere with a GFP/NHDFPF sphere or with another mCherry/MDAPF sphere in the same outer gel (Figure 3C). A significant increase in the migration index after 5 days of cell culture was observed only in the presence of the two mCherry/MDAPF spheres in the same outer gel. In Figure 3D, the cell migration index is shown.

It is not possible to have the spheres always at the same distance in different experimental replicates. However, this experimental variability in the distance between spheres may not be so relevant in the total effect observed considering the very small volume (98 μL), the highly diffusible soft material such as hydrogel, the long times for each experiment, and the experimental replicates.

Accordingly, no increase in MDAPF invasion was also observed when the fibroblasts were seeded on the bottom of the inner well as described in **Figure 4A**. In this case was observed a little reduction of the invasion of the MDAPF in the experiments performed with both normal or fluorescent cells (see Figure 4B,C). In Figure 4D the migration index is reported. This finding probably was due to a high cell proliferation of the fibroblasts on the bottom and a consequent release of the factors that increase the oxidative stress.

2.2.2. 3DCM-Chip of Co-Cultures for Monitoring the Effects of Biochemical and Physical Stimuli

In order to assess the possible relevance of major physical interactions between the different cell types and the synergic action of chemical and physical changes of the microenvironment in increasing the invasiveness of the MDAPF, the following conditions were assessed. In **Figure 5A** is shown the scheme of the condition in which the MDAPF sphere was embedded in outer gel with NHDFs.

In this case, a significant increase in the invasiveness of the cancer cells, ≈50% increase, was observed with respect to the condition in the absence of the fibroblasts in the outer gel (Figure 5B–D). In Figure 5B, a Hoechst 33342 live cell staining of the MDAPF sphere before its inclusion in the outer gel was performed. The observed increase in invasiveness could be explained by a substantial change, both chemical and physical, in the cellular environment. The presence of NHDFs in the external gel, in fact, could lead to proteolytic digestion of the external PF, driven by the release of metalloproteases (MMPs) from fibroblasts, resulting in a stiffness reduction and in the formation of an external gel with a molecular composition, which more closely resembles the ECM (e.g., higher presence of fibronectin), such as also demonstrated in other studies.[56–58]

The subsequent condition analyzed is in **Figure 6A**, where the cancer cells were in direct contact with the fibroblast. mCherry/MDA-MB 231 cells were embedded within the same sphere with GFP/NHDFs (Figure 6A,B).

This resulted in the formation of multi-cellular sphere (MDA-NHDFPF), which was then embedded into the outer gel. The invasion of cancer cells was monitored over time and compared to the situation where fibroblasts were absent. Interestingly, the presence of fibroblasts had a significant impact on outgrowth of MDA-MB 231 cells in these systems (Figure 6B and Video S1,

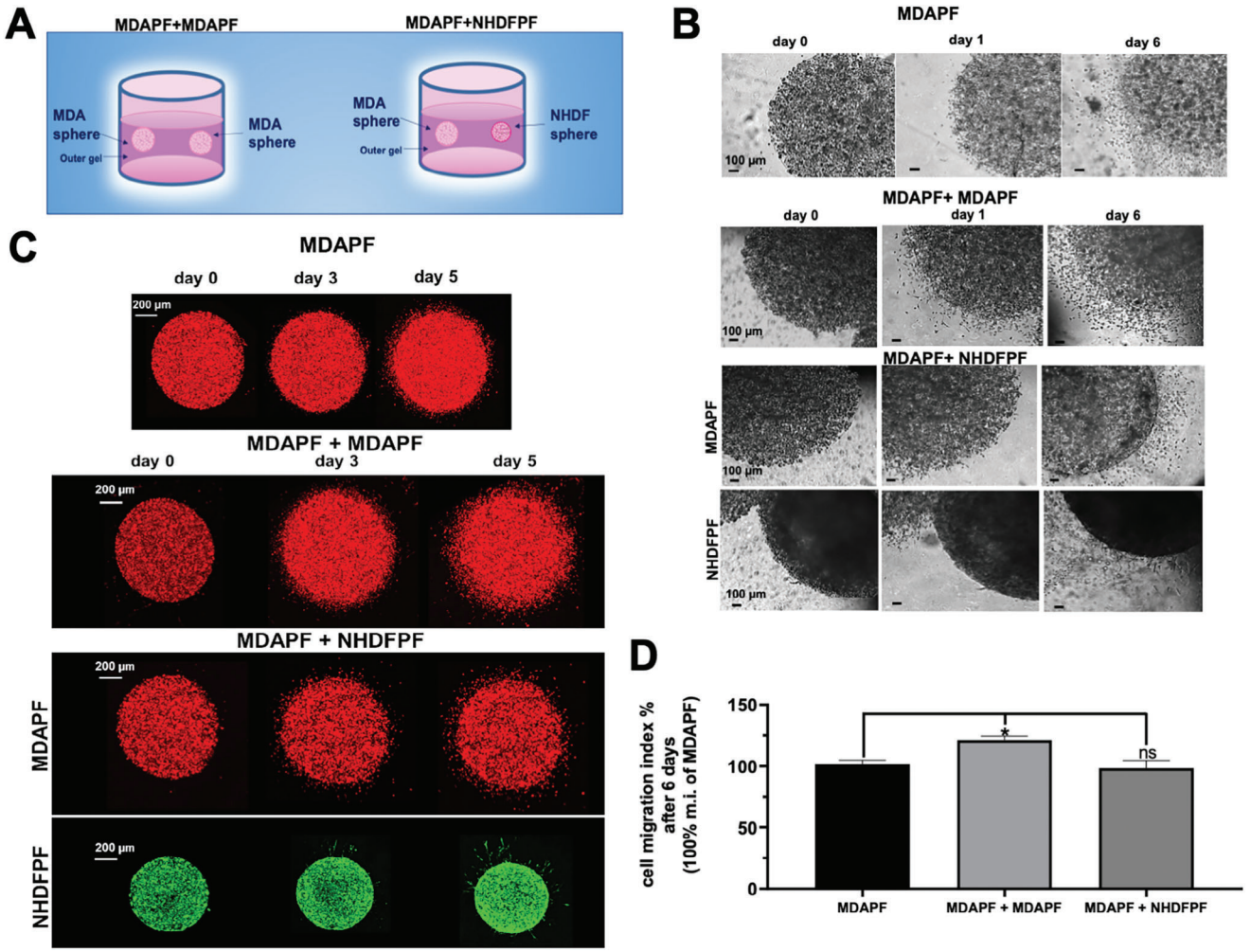

Figure 3. Effects of another MDAPF or of NHDFPF on the MDAPF tumoroid invasion. A) Schematic representation of the MDAPF in the gel-in-gel configuration with another MDAPF or with a NHDFPF embedded in the outer gel; B) brightfield micrographs and C) confocal micrographs of MDAPF invasion over time in the absence and in the presence of MDAPF (MDAPF + MDAPF) or of NHDFPF (MDAPF + NHDFPF). Cell density of spheres was 4×10^4 cells μL^{-1}. D) The cell migration index for each type of experiment after 6 days of cell cultures was calculated by three independent experiments. Error bar indicates S.D. *p-value ≤ 0.05 calculated using One-way ANOVA test. Scale bars are of 100 and 200 µm.

Supporting Information). The migration index calculated after 4 days of cell culture showed a substantial increase of 50% in breast cancer cells outgrowth in the presence of fibroblasts compared to the situation without fibroblasts (Figure 6C,D). Through a careful analysis of the fluorescence images obtained over time, it is also possible to observe that the presence of tumor cells leads to a significant reduction in the migration of NHDF within the external gel. Conversely, these NHDF cells exhibit a greater tendency to form a more compact sphere centrally. This compact cellular structure at the center of the MDA-NHDFPF sphere could indeed result in an internal increase of the stiffness, promoting the migration of tumor cells into the external gel. This speculation may be in agreement with the increase of the cancer cell invasiveness observed in breast cancer with microcalcifications,[53,59–61] and also with stromal fibrosis observed in most lung, breast, and pancreatic carcinomas.[62–66]

These experiments using 3DCM-chip shed light on the dynamic interactions between cancer cells and fibroblasts within the TME, furthering our understanding of the complex interplay in this microenvironment.

These findings indicate that the presence of fibroblasts, whether in the inner or outer gel, leads to an increase in tumor cell invasiveness. This aligns with existing literature, which reports that the presence of fibroblasts in the TME exerts a pro-invasive effect on tumor cells in various cancers.[67–70] This increased motility is likely attributed to a combination of biochemical and mechano-physical factors, with the latter being related to matrix remodeling and compositional changes promoted by the fibroblasts. It has been demonstrated that in the TME the fibroblasts transform into Cancer Associated Fibroblasts (CAFs), which are activated fibroblasts known to have a pro-invasive influence on tumor cells.[71,72] These findings offer valuable insights into

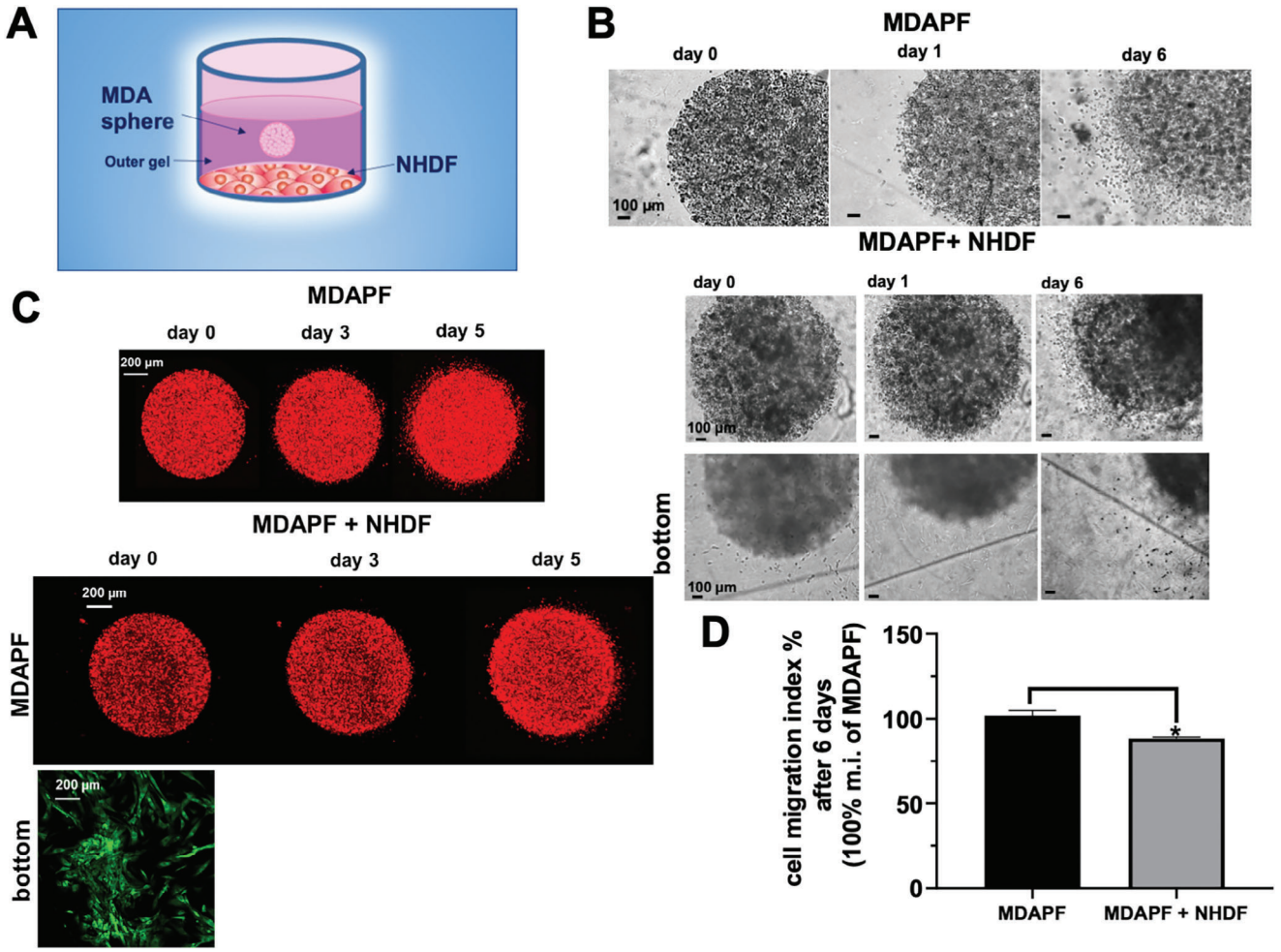

Figure 4. Effects of 2D seeded NHDFs on the MDAPF tumoroid invasion. A) Schematic representation of the MDAPF in the gel-in-gel configuration with NHDFs seeded on the bottom of the well; B) brightfield micrographs and C) confocal micrographs of MDAPF (cell density of 4×10^4 cells μL^{-1}) invasion over time in the absence and in the presence of NHDFs (MDAPF + NHDF), NHDFs seeded at a cell density of 2×10^4 cells cm^{-2}; D) migration index after 6 days of cell culture was calculated by three biological replicates. Error bar indicates S.D. *p-value ≤ 0.05 calculated using t-test. Scale bars are 100 and 200 µm.

the complex interactions within the TME and the role of fibroblasts in influencing tumor cell behavior.

2.3. CAFs Trans-Differentiation of NHDFs Induced by MDAPF

In light of our previous observations, we performed a deep analysis to assess whether fibroblasts within our model underwent trans-differentiation into CAFs when exposed to breast cancer cells. The CAF transformation, in fact, can contribute to the promotion of tumor invasion as described in several studies.[73,74] CAFs promote tumor progression, ECM remodeling, inflammation, chemoresistance, and immunosuppression.[75–77]

The specific origin of different subtypes of CAFs in breast cancer is not fully understood although it is reported that tumor-secreted factors are crucial in controlling CAF-precursors' differentiation in CAFs.[78]

Recently, some emerging studies have described the biology, origin, and function of CAFs and how their targeting is being explored to improve the outcome of anti-cancer therapies, although targeting CAFs results are particularly challenging, due to the extremely heterogeneous nature of these cells. Therefore, to explore the hypothesis that fibroblasts underwent trans-differentiation into CAFs when exposed to MDAPF, we seeded NHDFs onto a tissue culture plate and co-cultured them for 1 week in the presence of MDAPF.

In **Figure** 7A is shown the crystal violet staining of the NHDFs cultured in the presence and in the absence of MDAPF. NHDFs cultured in the presence of MDAPF show an altered dimension with a more elongated and spindled cell morphology. This morphology is typically associated with a CAF-like phenotype.[79] Therefore, the expression of the protein α-smooth muscle actin (α-SMA), one of the primary biomarkers of CAFs,[80–84] in NHDFs cultured for 4 days in the presence of MDAPF was assessed. By immunofluorescence analysis, it was evident that NHDFs grown in the presence of tumor cells, especially in close proximity to the sphere, exhibited higher α-SMA protein expression compared to NHDFs cultured in isolation (Figure 7B and Figure S1,

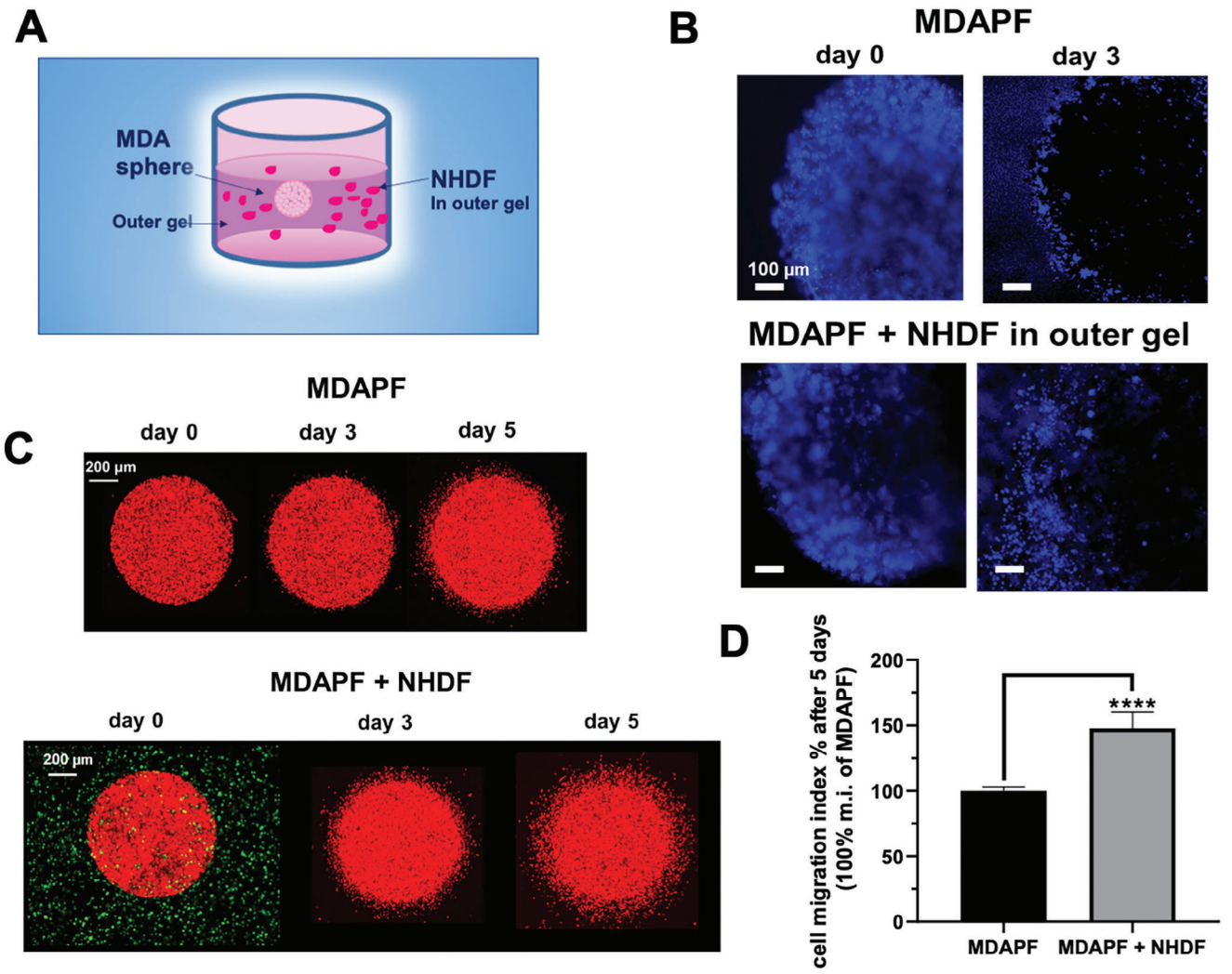

Figure 5. 3DCM-chip for analyzing the effects of NHDFs on the MDAPF tumoroid invasion. A) Schematic representation of the MDAPF in the gel-in-gel configuration with NHDFs embedded in the outer gel; B) fluorescence micrographs of the invasion of MDAPF pre-stained with Hoechst 33342 (staining of the nuclei of live cells), in the absence and in the presence of NHDFs in the outer gel (NHDFs embedded at a cell density of 2×10^4 cells μL^{-1}); C) confocal micrographs of MDAPF invasion over time in the absence and in the presence of NHDFs in the outer gel; D) cell migration index after 5 days of cell culture evaluated by four independent biological replicates. Error bar indicates S.D. ****p-value $\leq$ 0.0001 calculated using t-test. Scale bars are 100 and 200 µm.

Supporting Information). This observation was corroborated by quantitative protein expression evaluation using western blot analysis (Figure 7C). Furthermore, a statistically significant increase in the expression of cyclin D1 and of the active form of Akt protein (p-Akt) (protein kinase B) was detected in NHDFs co-cultured with MDAPF (Figure 7C). This finding aligns with recent research indicating that stromal cancer-associated fibroblasts express high levels of cyclin D1 in vivo.[85] Therefore, the increase in invasiveness of MDAPF tumor cells, observed in the presence of NHDFs either in the outer or inner gel, can be explained by a transformation of NHDFs into CAFs combined with the subsequent chemical-physical remodeling of the TME.

CAFs are reported to release a range of substances, including metalloproteinases like MMP2 and MMP9, which contribute to the remodeling of the ECM.[86] Additionally, CAFs release growth factors and cytokines such as C-C motif chemokine ligand 7 (CCL7), transforming growth factor beta (TGFβ), and stromal cell-derived factor 1 (SDF-1). These molecular signals collectively play a significant role in promoting various aspects of tumor behavior, including proliferation, spreading, aggressiveness, and angiogenesis.[87–92] Recognizing these intricate dynamics is essential for the development of precise and targeted therapeutic approaches in the treatment of cancer. By gaining insights into how CAFs and their secreted molecules influence the TME, it is possible to identify potential therapeutic targets to arrest the progression of cancer and enhance the effectiveness of treatment strategies.[76,93]

Therefore, the results here reported are consistent with existing literature,[67–70,94] validating our 3D co-culture systems as reliable in vitro models capable of potentially recapitulating important aspects of the cross-talk between cancer cells and stromal cells in their microenvironment in vivo.

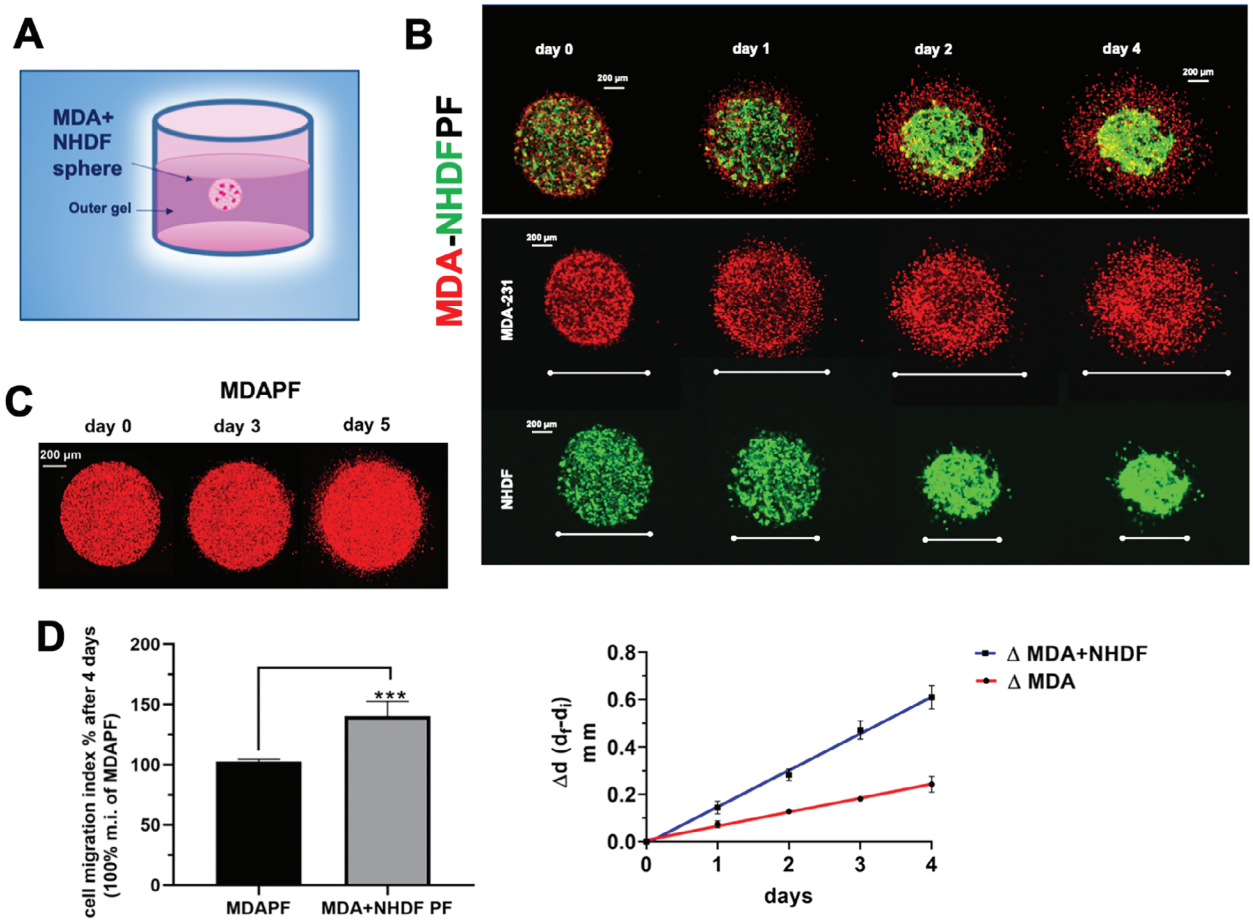

Figure 6. 3DCM-chip: effects on MDA-MB 231 cells invasion in MDA-NHDFPF system. A) Schematic representation of the tumoroid embedding MDA-MB 231 cells and NHDFs, in the gel-in-gel configuration; B) confocal micrographs of the MDA-MB 231 cells and NHDFs tumoroid (MDA-NHDFPF) invasion over time (cell density of MDA-MB 231 and of NHDFs of 2×10^4 cells μL^{-1}); C) mCherry/MDAPF invasion over time without NHDFs; D) cell migration index after 4 days of cell culture and linear regression of the differences between the sphere diameters (Δd ($d_f - d_i$)) measured over time for the MDAPF tumoroid in the presence and in the absence of NHDFs. These results are obtained by three independent biological replicates. Error bar indicates S.D. ***p-value $\leq$ 0.0005 obtained by t-test. Scale bars are of 200 µm.

2.4. More Complex 3D Systems: MDA-MSCPF with NHDFs and HUVECs in the Outer Gel

Finally, we assessed the potentiality of the 3DCM-chip in the analysis of more complex systems. In **Figure** 8A is shown the scheme of the analyzed condition, where a sphere with cancer and mesenchymal stem cells (MDA-MSCPF) was produced and embedded into an external gel with both HUVECs and NHDFs.

This 3D cellular model could better simulate the physiologic condition and allow to analyze the effects of several cells in 3D more complex systems. In agreement with the case shown in Figure 5, the cancer cells of the MDA-MSCPF sphere were more able to invade the outer gel (Figure 8C) and the presence of MDA-MSCPF sphere stimulated the formation of tubular constructs of HUVECs (Figure 8D) that were not obtained in the absence of the sphere (Figure 8E). The formation of these microvascular structures opens the way to investigate the pro-angiogenic activity of the cancer cells using this platform.

The microvascular formation was 4.5 mm in length with a diameter of 150 µm. Moreover, from a careful analysis of the cellular construct, it is also possible to highlight the presence of mCherry/MDA-MB 231 cells within the tubular structure formed by GFP/HUVECs after 6 and 7 days of cell growth (Figure 8D).

A critical step of the tumor progression is the intravasation of the cancer cells, which cross endothelial barriers to enter the circulatory or lymphatic systems leading to metastatization.[92,95,96] Understanding and targeting the mechanisms involved in intravasation could be pivotal in developing strategies to impede or control the metastatic spread of cancer.

These preliminary studies demonstrate that our platform could allow to create models for evaluating not only the rate of cell migration and growth, but also the angiogenic potential and the intravasation of a tumor.

3. Conclusions

Here, the design, production, and potential applications of the 3DCM-chip for the gel-in-gel cell migration/invasion assay have been described. This device offers a range of advantages and possibilities for the study of cell migration/invasion in dependence

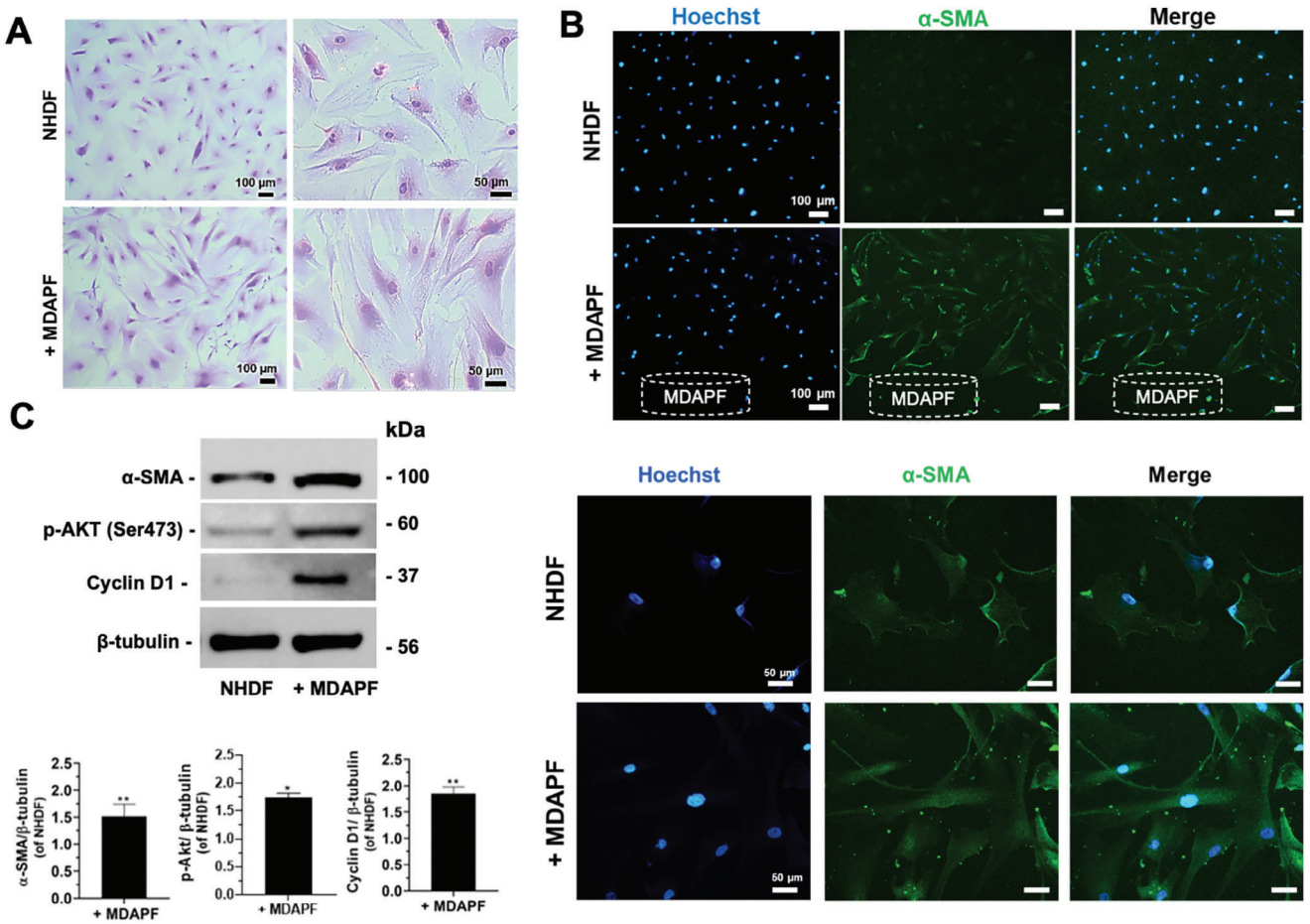

Figure 7. NHDFs activation to CAFs by co-culturing with MDAPF tumoroid. A) Brightfield micrographs of NHDFs (seeded at a cell density of 10^4 cells cm^{-2}) in the absence and in the presence of MDAPF (cell density of 10^4 cells μL^{-1}) after 7 days of cell co-culture, stained with crystal violet; B) fluorescence micrographs of NHDFs grown in the absence and in the presence of MDAPF for 4 days. Cell nuclei are stained with Hoechst 33342 and α-SMA is stained in green. Scale bars are of 100 and 50 µm; C) p-Akt, α-SMA, and Cyclin D1 expression assessed by western blot analysis of NHDFs cultured with and without MDAPF for 3 days. Blots are representative experiments of three biological replicates. ImageJ software was used to perform the densitometric analysis of the protein bands. Error bars indicate S.D. *p-value ≤ 0.05, **p-value ≤ 0.01 calculated using t-test.

on chemical and physical changes of the microenvironment and to analyze in detail the effects of different cells in complex co-culture systems. The key benefits and features of our innovative microfluidic device can be summarized here: i) 3DCM-chip provides a 3D system for studying cell migration and invasiveness, allowing for better mimicry of physiological conditions; ii) it uses micro-quantities of cells and reagents, which not only reduces costs but also makes the system more practical and user-friendly (see Video S2, Supporting Information); iii) it enhances experimental reproducibility, ensuring consistent results across different trials; iv) the chip's design allows for easy media changes, washing, solution replacements, and the addition of compounds or drugs. Channels within the chip facilitate these processes without risking damage to the system; v) the internal well's surface can be easily modified to become super-hydrophobic, making the device suitable for various types of polymers; vi) the transparency of the chip's polymer material enables cellular microscopic analyses, including optical microscopy and fluorescence microscopy. This ensures quick and accurate observations without sample alterations during preparation; vii) it allows to perform biochemical assays and western blotting analyses and simultaneous study of multiple replicates, which is crucial for statistical evaluation; viii) the chip is designed in a way that makes it compatible with "multiplates" allowing for scalability and increased throughput; ix) 3DCM-chip can be realized through various additive/subtractive manufacturing techniques, offering flexibility in its production; x) super-hydrophobic materials can be directly applied to the chip, further enhancing its capabilities and versatility; xi) finally, this device can be useful to perform co-culture systems, as here demonstrated, and to better study the TME. There is a lack of studies that specifically delve into unraveling the metastatic behavior of the different cancer types, and additional efforts are needed to comprehend and reproduce the key components of the TME in the different tumors.

Further, implementation and optimization of this device could also lead in the next future to the production of an in vitro organotypic model of the stem niche, where adult stem cells (ASCs) are found. In these crypts, whose presence has been found in numerous tissues and organs of the adult individual, such as the endothelium, skeletal and cardiac muscle, liver, and cornea,

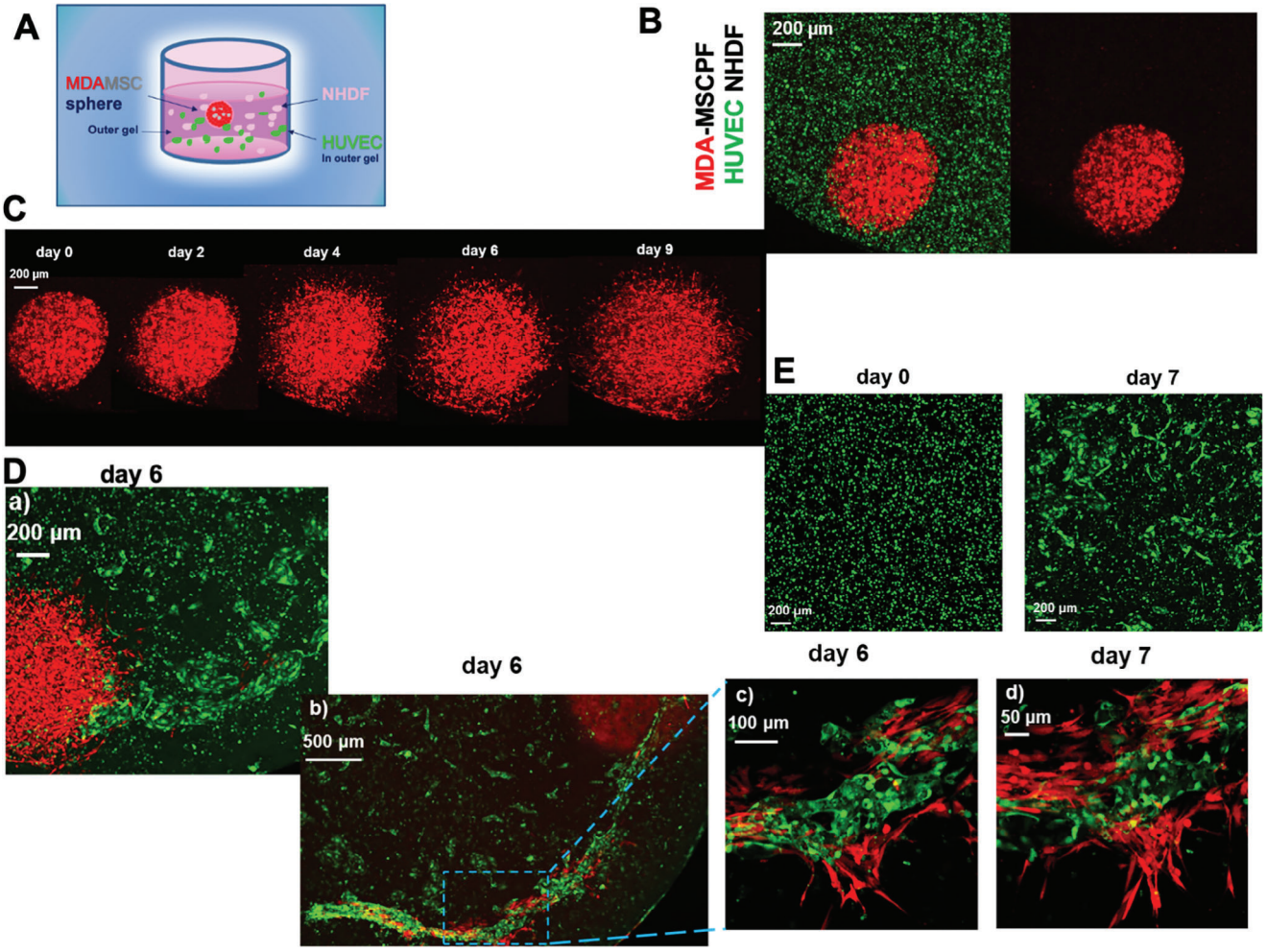

Figure 8. 3DCM-chip for the modeling of more complex systems: MDA-MSCPF with NHDFs and HUVEC cells embedded in outer gel. A) Schematic representation of the tumoroid embedding mCherry/MDA-MB 231cells and MSCs, in the gel-in-gel system with NHDFs and GFP/HUVECs in the outer gel; B) confocal micrographs of the mCherry/MDA-MB 231cells and MSCs tumoroid (MDA-MSCPF) at day 0 with GFP/HUVECs and NHDFs in the outer gel; C) confocal micrographs of the MDA-MSCPF invasion over time; D) vessels-like structures formation after 6 days of cell culture and intravasation of tumor cells inside the vessels; E) confocal micrographs of GFP/HUVECs and NHDFs cells, with a cell density of 85×10^3 cells mL^{-1} and 17×10^3 cells mL^{-1} respectively, cultured in PFHy using the composition of the outer gel at day 0 and after 7 days of growth. Micrographs are representative of three independent biological replicates. Scale bars are of 50, 100, 200, and 500 µm.

the ASCs remain confined and relatively quiescent until reactivated by damages or diseases. Therefore, 3DCM-chip may allow the exploitation of the gel-in-gel assay, until now used only in the context of cancer investigation, also in the field of regenerative medicine, creating in vitro models for investigating physicochemical stimuli effects on stem cells migration ability during stem cells delivery and transplantation in the host damaged tissue.

4. Experimental Section

3DCM-Chip Fabrication: The 3DCM-chip has been created as described in the Italian patent.[34] Briefly, the realization of the chip has been carried out using polystyrene combined with extruded and cast PMMA, an optimal material to give the chip a good transparency in order to be able to carry out subsequent microscopic analyses. The chip was characterized by microfluidics systems able to facilitate and make the preparation of the system by the operator extremely reproducible, allowing also the use of smaller quantities of cells and reagents that were usually very expensive. The chip was made of an internal well that contains the gel-in-gel system, a removable nanostructured super-hydrophobic surface,[35,53] and two channels: a bottom channel for washing the cellular microsphere (inner gel with cells) and removing the cells not included in the microsphere; an upper channel for washing the gel-in-gel system, and the external well containing the culture medium. The chip was designed in Autodesk Inventor and fabricated with a laser cut machine (Trotec Laser GmbH, Austria). The layers were aligned together with a custom aluminum holder and assembled with a double-sided adhesive (467 MP transfer tape 3M Maplewood, US) by pressing at 100 bar for 3 min with a hydraulic press (Beta 3027-10, Beta Utensili s.p.a.).

Cell Cultures and Cell PF Spheres Production: The following cell lines were used: human cardiac Sca-1^+ Lin^- MSCs (cMSCs) that were isolated from auricular biopsies taken during coronary artery bypass surgery, as described elsewhere,[97] MDA-MB 231, NHDFs, BM-MSCs, mCherry/MDA-MB 231, GFP/NHDFs and GFP/HUVECs (Lonza, Basel, Switzerland).

These cell lines were cultured in Dulbecco's modified Eagle medium (DMEM) (Gibco, Thermo Fisher Scientific, Milan, Italy) supplemented with 10% of fetal bovine serum (FBS) (v/v) (Gibco, Thermo Fisher Scientific, Milan, Italy), 2 mM L-Glutamine, 100 U mL^{-1} penicillin, and 100 µg mL^{-1} streptomycin (complete medium) at 37 °C and with 5% CO_2.

For the cell microsphere production, after detachment by treatment with trypsin EDTA, the cells were washed with PBS and resuspended in PF hydrogel precursor solution at a cell density of 4×10^4 cells μL^{-1}. The PFHy precursor solution was obtained according to a published protocol.[28,33,98] Briefly, the PFHy precursor solution was solubilized in PBS, pH 7.4, at a final concentration of 8 mg mL^{-1} of PF, and to favor the gelation process, 0.5% v/v PEGDA (10 kDa) of a 30% PEGDA solution was also added. The assembly of PFHy was achieved via free-radical polymerization by adding 1% v/v of a photo-initiator stock solution containing 10% w/v Irgacure 2959 (Ciba Specialty Chemicals, Basel, Switzerland) in 70 vol% ethanol; thus, the gelation occurred by exposing the microspheres dropped on a nanostructured super-hydrophobic surface to UV light (365 nm, 4–5 mW cm^{-2}) for 2 min. The superhydrophobic surface of PDMS was here fabricated with nano-structures using the procedure described by Patent LDO0252.[35] The cell-loaded PF microspheres were cultivated in a complete medium. After 24 h of cell growth, the PF spheres were embedded in the outer gel precursor solution (at a final concentration of 5.5 mg mL^{-1} of PF in PBS pH 7.4) exposing to UV light (365 nm, 4–5 mW cm^{-2}) for 5 min to allow the outer gel photopolymerization.

Optical and Fluorescence Microscopy Analyses: Cellular invasion of the PF spheres in the 3DCM-chip was monitored over time by brightfield and fluorescence microscopy using a Zeiss Axio Observer 7 microscope and a Zeiss LSM 700 confocal microscope, respectively. The cell outgrowth was visualized also using the time-lapse microscopy, capturing images every 4 h for 4 days in culture using a 5× objective and a custom-built microscope system maintaining the chip inside an incubated environmental chamber with a temperature controller (37 °C and 5% CO_2). Fluorescence microscopy of MDAPF spheres was also performed by nuclei staining of live cells with Hoechst 33342 (Sigma Aldrich, Italy) prior to their encapsulation in the outer gel. Immunofluorescence analysis of NHDFs grown in the presence of MDAPFs was performed by fixing the cells with 4% paraformaldehyde in PBS for 30 min at room temperature, then permeabilizing with 0.3% Triton X-100 for 5 min, and maintaining in a blocking buffer (10% v/v FBS, 0.1% v/v Triton X-100, and 1% w/v glycine in PBS) overnight at 4 °C. Samples were then incubated overnight at 4 °C with 1:200 v/v Ab-α-SMA (Thermo Fisher Scientific, Invitrogen, USA) in PBS with 1% albumin, 20 mM Gly solution, followed by 3 h of incubation with the appropriate 1:200 v/v Alexa488 fluorochrome-conjugated secondary antibody in 20 mM Gly-PBS at room temperature. After, cell nuclei were stained with Hoechst 33342. Fluorescence micrographs were captured using a Zeiss Axio Observer 7 microscope. NHDFs grown in the presence of MDAPF were also observed by Crystal Violet staining using a Zeiss Primovert optical microscope.

Western Blot Analysis: Protein extraction from NHDFs grown in the presence of MDAPF was performed using RIPA buffer (100 µL) containing a protease inhibitor cocktail (Sigma Aldrich, Milan, Italy) and pervanadate (Sigma Aldrich, Italy) as a phosphatase inhibitor. After incubation for 90 min in ice, lysates were centrifuged for 10 min at 8000 rpm at 4 °C. BCA protein assay (Sigma Aldrich, Milan, Italy) was used to determine the protein content, and the SDS-PAGE of cell extracts (30 µg of protein) was performed using 12% polyacrylamide gel. For electro-blotting, PVDF membranes (Sigma Aldrich, Italy) were used and were then blocked and probed with primary monoclonal antibodies Ab-p-Akt rabbit (Cell Signaling Technology, USA), Ab-α-SMA (Thermo Fisher Scientific, Invitrogen, USA), Ab-Cyclin D1 rabbit (Cell Signaling Technology, USA). Immunoblots were next incubated with the secondary antibodies (dilution 1:3000) (Cell Signaling Technology, USA) for 4 h at room temperature. Immunoblot with Ab-β-tubulin mouse (Sigma Aldrich, Milan Italy) were also probed for controlling the protein loading. A Super Signal West Pico kit (Thermo Scientific, USA) was used to visualize the signal, followed by exposure to a Fluorchem Imaging system (Alpha Innotech Corporation-Analitica De Mori, Milan, Italy). ImageJ software was used to perform the densitometric analysis of the protein bands of three independent biological replicates.

Statistical Analysis: GraphPad Software (GraphPad Prism version 5.0, San Diego, CA, USA) was used to perform statistical analyses on data obtained from three or more experimental biological replicates. Each variable was quantified and analyzed using *t*-test or One-way ANOVA-test followed by Dunnett's multiple comparisons test. A *p*-value < 0.05 was considered statistically significant. Standard deviations were calculated using three or four biological replicates and presented for each type of experiment.

Supporting Information

Supporting Information is available from the Wiley Online Library or from the author.

Acknowledgements

The authors thank Ilaria Arciero, Stefano Eriani, and the Shulamit Levenberg's group for their technical support in some experiments. The research leading to these results has received funding from the European Union-Next Generation EU through the Italian Ministry of University and Research under PNRR–M4C2-I1.3 Project PE_00000019 "HEAL ITALIA." This research was partially supported by the Israel Science Foundation grant no. 2130/19. The views and opinions expressed are those of the authors only and do not necessarily reflect those of the European Union or the European Commission. Neither the European Union nor the European Commission can be held responsible for them.

Conflict of Interest

The authors declare no conflict of interest.

Data Availability Statement

The data that support the findings of this study are available from the corresponding author upon reasonable request.

Keywords

breast cancer, cancer associated fibroblasts, cellular invasion, co-cultures, HUVECs, lab on a chip, PEG-fibrinogen, stem cells

Received: January 4, 2024
Revised: April 24, 2024
Published online:

[1] J. K. Lee, D. M. Havaleshko, H. Cho, J. N. Weinstein, E. P. Kaldjian, J. Karpovich, A. Grimshaw, D. Theodorescu, *Proc. Natl. Acad. Sci. USA* **2007**, *104*, 13086.
[2] L. J. Van't Veer, R. Bernards, *Nature* **2008**, *452*, 564.
[3] K. H. Benam, S. Dauth, B. Hassell, A. Herland, A. Jain, K.-J. Jang, K. Karalis, H. J. Kim, L. MacQueen, R. Mahmoodian, S. Musah, Y. Torisawa, A. D. van der Meer, R. Villenave, M. Yadid, K. K. Parker, D. E. Ingber, *Annu. Rev. Pathol.: Mech. Dis.* **2015**, *10*, 195.
[4] P. Mehta, Z. Rahman, P. ten Dijke, P. E. Boukany, *Trends Cancer* **2022**, *8*, 683.
[5] F. Hirschhaeuser, H. Menne, C. Dittfeld, J. West, W. Mueller-Klieser, L. A. Kunz-Schughart, *J. Biotechnol.* **2010**, *148*, 3.
[6] M. P. Lutolf, J. Hubbell, *Nat. Biotechnol.* **2005**, *23*, 47.
[7] A. M. Kloxin, A. M. Kasko, C. N. Salinas, K. S. Anseth, *Science* **2009**, *324*, 59.

[8] D. Seliktar, *Science* **2012**, *336*, 1124.
[9] M. Mirbagheri, V. Adibnia, B. R. Hughes, S. D. Waldman, X. Banquy, D. K. Hwang, *Mater. Horiz.* **2019**, *6*, 45.
[10] T.-C. Tang, B. An, Y. Huang, S. Vasikaran, Y. Wang, X. Jiang, T. K. Lu, C. Zhong, *Nat. Rev. Mater.* **2021**, *6*, 332.
[11] C. Nurchi, S. Buonvino, I. Arciero, S. Melino, *Int. J. Mol. Sci.* **2023**, *24*, 2153.
[12] X. Trepat, Z. Chen, K. Jacobson, in *Comprehensive Physiology* (Ed: R. Terjung), Wiley, Hoboken, NJ **2012**, pp. 2369–2392.
[13] A. D. Doyle, N. Carvajal, A. Jin, K. Matsumoto, K. M. Yamada, *Nat. Commun.* **2015**, *6*, 8720.
[14] A. A. Solbu, D. Caballero, S. Damigos, S. C. Kundu, R. L. Reis, Ø. Halaas, A. S. Chahal, B. L. Strand, *Mater Today Bio* **2023**, *18*, 100537.
[15] N. Blow, *Nat. Methods* **2007**, *4*, 589.
[16] L. R. Johnson, K. E. Barrett, *Physiology of the Gastrointestinal Tract*, Academic Press, Cambridge, MA **2006**.
[17] K. Schroeder, B. D. Neagle, *Essen Bioscience Inc. USA Patent N: 5,210,021 and 5,302,515*, **1994**.
[18] F. Zheng, F. Fu, Y. Cheng, C. Wang, Y. Zhao, Z. Gu, *Small* **2016**, *12*, 2253.
[19] J. H. Kim, Y.-J. Seol, I. K. Ko, H.-W. Kang, Y. K. Lee, J. J. Yoo, A. Atala, S. J. Lee, *Sci. Rep.* **2018**, *8*, 12307.
[20] J. Aleman, S. K. George, S. Herberg, M. Devarasetty, C. D. Porada, A. Skardal, G. Almeida-Porada, *Small* **2019**, *15*, 1902971.
[21] S. Ostrovidov, S. Salehi, M. Costantini, K. Suthiwanich, M. Ebrahimi, R. B. Sadeghian, T. Fujie, X. Shi, S. Cannata, C. Gargioli, A. Tamayol, M. R. Dokmeci, G. Orive, W. Swieszkowski, A. Khademhosseini, *Small* **2019**, *15*, 1805530.
[22] J. Ruiz-Espigares, D. Nieto, L. Moroni, G. Jiménez, J. A. Marchal, *Small* **2021**, *17*, 2006009.
[23] R. Rodriguez-Moncayo, A. M. Gonzalez-Suarez, O. López-Ortega, J. L. Garcia-Cordero, in *Cell Movement in Health and Disease* (Eds: M. Schnoor, L.-M. Yin, S. X. Sun), Academic Press, Cambridge, MA **2022**, pp. 273–293.
[24] J. Ren, N. Wang, P. Guo, Y. Fan, F. Lin, J. Wu, *Lab Chip* **2022**, *22*, 3361.
[25] B. Sharma, A. Sharma, *Adv. Eng. Mater.* **2022**, *24*, 2100738.
[26] S. Ye, Q. Cao, P. Ni, S. Xiong, M. Zhong, T. Yuan, J. Shan, J. Liang, Y. Fan, X. Zhang, *Small* **2023**, *19*, 2302152.
[27] E. Ivanir, Y. Shachaf, I. Mironi-Harpaz, D. Yeheskely-Hayon, L. Hazanov, S. Harpaz-Segev, T. Birman, L. Minai, S. Melino, D. Yelin, D. Seliktar, *Adv. Funct. Mater.* **2020**, *30*, 1807106.
[28] S. Buonvino, M. Ciocci, D. Seliktar, S. Melino, *Int. J. Mol. Sci.* **2021**, *22*, 6095.
[29] N. Cohen, Y. Vagima, O. Mouhadeb, E. Toister, H. Gutman, S. Lazar, A. Jayson, A. Artzy-Schnirman, J. Sznitman, A. Ordentlich, S. Yitzhaki, D. Seliktar, E. Mamroud, E. Epstein, *Front Bioeng Biotechnol* **2022**, *10*, 905557.
[30] Y. Berkovitch, D. Seliktar, *Int. J. Pharm.* **2017**, *523*, 545.
[31] A. Yosef, O. Kossover, I. Mironi-Harpaz, A. Mauretti, S. Melino, J. Mizrahi, D. Seliktar, *Adv. Healthcare Mater.* **2019**, *8*, 1801436.
[32] M. Ciocci, I. Cacciotti, D. Seliktar, S. Melino, *Int. J. Biol. Macromol.* **2018**, *108*, 960.
[33] L. Almany, D. Seliktar, *Biomaterials* **2005**, *26*, 2467.
[34] S. Melino, D. Seliktar, E. Martinelli, S. Buonvino, D. Di Giuseppe, *Italian Patent N: 102021000025460*, **2023**.
[35] A. Garibbo, C. Boragno, F. Gagliardi, *US20120181717A1*, **2019**.
[36] R. Lanza, N. Rosenthal, *Sci. Am.* **2004**, *290*, 92.
[37] S. J. Morrison, A. C. Spradling, *Cell* **2008**, *132*, 598.
[38] J. F. Gil, C. S. Moura, V. Silverio, G. Gonçalves, H. A. Santos, *Adv. Mater.* **2023**, *35*, 2300692.
[39] G. Tang, L. Wu, W. Liang, R. Wang, *Mol. Pharmacol.* **2005**, *68*, 1757.
[40] U. Sen, P. K. Mishra, N. Tyagi, S. C. Tyagi, *Cell Biochem. Biophys.* **2010**, *57*, 49.
[41] K. Eto, T. Asada, K. Arima, T. Makifuchi, H. Kimura, *Biochem. Biophys. Res. Commun.* **2002**, *293*, 1485.
[42] J. L. Wallace, R. Wang, *Nat. Rev. Drug Discovery* **2015**, *14*, 329.
[43] S. A. Mard, N. Neisi, G. Solgi, M. Hassanpour, M. Darbor, M. Maleki, *Dig Dis Sci* **2012**, *57*, 1496.
[44] M. V. Chan, J. L. Wallace, *Am. J. Physiol.: Gastrointest. Liver Physiol.* **2013**, *305*, G467.
[45] Z. W. Lee, J. Zhou, C.-S. Chen, Y. Zhao, C.-H. Tan, L. Li, P. K. Moore, L.-W. Deng, *PLoS One* **2011**, *6*, e21077.
[46] Q. Dong, B. Yang, J.-G. Han, M.-M. Zhang, W. Liu, X. Zhang, H.-L. Yu, Z.-G. Liu, S.-H. Zhang, T. Li, D.-D. Wu, X.-Y. Ji, S.-F. Duan, *Cancer Lett* **2019**, *455*, 60.
[47] S. Sakuma, S. Minamino, M. Takase, Y. Ishiyama, H. Hosokura, T. Kohda, Y. Ikeda, Y. Fujimoto, *Heliyon* **2019**, *5*, 8.
[48] E. E. Ngowi, A. Afzal, M. Sarfraz, S. Khattak, S. U. Zaman, N. H. Khan, T. Li, Q.-Y. Jiang, X. Zhang, S.-F. Duan, *Int J Biol Sci* **2021**, *17*, 73.
[49] A. I. Bhuiyan, V. T. Papajani, M. Paci, S. Melino, *Molecules* **2015**, *20*, 1731.
[50] Y. Liu, P. Zhu, Y. Wang, Z. Wei, L. Tao, Z. Zhu, X. Sheng, S. Wang, J. Ruan, Z. Liu, *PLoS One* **2015**, *10*, e0123781.
[51] M. Ciocci, E. Iorio, F. Carotenuto, H. A. Khashoggi, F. Nanni, S. Melino, *OncoTargets Ther.* **2016**, *7*, 51.
[52] X. Xie, X. Huang, H. Tang, F. Ye, L. Yang, X. Guo, Z. Tian, X. Xie, C. Peng, X. Xie, *Curr. Cancer Drug Targets* **2018**, *18*, 592.
[53] S. Buonvino, I. Arciero, E. Martinelli, D. Seliktar, S. Melino, *Mater Today Bio* **2023**, *23*, 100862.
[54] I. Cacciotti, M. Ciocci, E. Di Giovanni, F. Nanni, S. Melino, *Int. J. Mol. Sci.* **2018**, *19*, 2368.
[55] E. Di Giovanni, S. Buonvino, I. Amelio, S. Melino, *Int. J. Mol. Sci.* **2020**, *21*, 1638.
[56] S. I. Montanez-Sauri, K. E. Sung, E. Berthier, D. J. Beebe, *Integr. Biol.* **2013**, *5*, 631.
[57] F. Gioiella, F. Urciuolo, G. Imparato, V. Brancato, P. A. Netti, *Adv. Healthcare Mater.* **2016**, *5*, 3074.
[58] K. M. Lugo-Cintrón, M. M. Gong, J. M. Ayuso, L. A. Tomko, D. J. Beebe, M. Virumbrales-Muñoz, S. M. Ponik, *Cancers* **2020**, *12*, 1173.
[59] M. Scimeca, R. Bonfiglio, E. Menichini, L. Albonici, N. Urbano, M. T. De Caro, A. Mauriello, O. Schillaci, A. Gambacurta, E. Bonanno, *Int. J. Mol. Sci.* **2019**, *20*, 5633.
[60] S. Kim, T. X. M. Tran, H. Song, B. Park, *Breast Cancer Res.* **2022**, *24*, 96.
[61] Y. Tian, L. Zhao, Z. Gui, S. Liu, C. Liu, T. Yu, L. Zhang, *Cancer Med.* **2023**, *12*, 11351.
[62] H. Sartor, S. Zackrisson, K. Elebro, L. Hartman, S. Borgquist, *Cancer Causes Control* **2015**, *26*, 931.
[63] M. S. Rice, K. A. Bertrand, T. J. VanderWeele, B. A. Rosner, X. Liao, H.-O. Adami, R. M. Tamimi, *Breast Cancer Res.* **2016**, *18*, 94.
[64] S. S. Nazari, P. Mukherjee, *Breast Cancer* **2018**, *25*, 259.
[65] L. P. Hariri, D. C. Adams, M. B. Applegate, A. J. Miller, B. W. Roop, M. Villiger, B. E. Bouma, M. J. Suter, *Clin. Cancer Res.* **2019**, *25*, 5242.
[66] B. Sajjad, N. Farooqi, B. Rehman, I. B. Khalid, N. Urooj, S. Sajjad, A. Mumtaz, T. Tariq, A. Iqbal khan, M. A. Parvaiz, *Cureus* **2022**, *14*, e27028.
[67] M. E. Fiori, S. Di Franco, L. Villanova, P. Bianca, G. Stassi, R. De Maria, *Mol Cancer* **2019**, *18*, 70.
[68] P. De, J. Aske, N. Dey, *Cancers* **2021**, *13*, 5246.
[69] D. Hu, Z. Li, B. Zheng, X. Lin, Y. Pan, P. Gong, W. Zhuo, Y. Hu, C. Chen, L. Chen, J. Zhou, L. Wang, *Cancer Commun* **2022**, *42*, 401.
[70] M. Sarkar, T. Nguyen, E. Gundre, O. Ogunlusi, M. El-Sobky, B. Giri, T. R. Sarkar, *Front Cell Dev Biol* **2023**, *11*, 1089068.
[71] E. Sahai, I. Astsaturov, E. Cukierman, D. G. DeNardo, M. Egeblad, R. M. Evans, D. Fearon, F. R. Greten, S. R. Hingorani, T. Hunter, R. O. Hynes, R. K. Jain, T. Janowitz, C. Jorgensen, A. C. Kimmelman, M. G. Kolonin, R. G. Maki, R. S. Powers, E. Puré, D. C. Ramirez, R. Scherz-

Shouval, M. H. Sherman, S. Stewart, T. D. Tlsty, D. A. Tuveson, F. M. Watt, V. Weaver, A. T. Weeraratna, Z. Werb, *Nat. Rev. Cancer* **2020**, *20*, 174.
[72] Q. Ping, R. Yan, X. Cheng, W. Wang, Y. Zhong, Z. Hou, Y. Shi, C. Wang, R. Li, *Cancer Gene Ther.* **2021**, *28*, 984.
[73] J. G. Goetz, S. Minguet, I. Navarro-Lérida, J. J. Lazcano, R. Samaniego, E. Calvo, M. Tello, T. Osteso-Ibáñez, T. Pellinen, A. Echarri, A. Cerezo, A. J. P. Klein-Szanto, R. Garcia, P. J. Keely, P. Sánchez-Mateos, E. Cukierman, M. A. Del Pozo, *Cell* **2011**, *146*, 148.
[74] F. Calvo, N. Ege, A. Grande-Garcia, S. Hooper, R. P. Jenkins, S. I. Chaudhry, K. Harrington, P. Williamson, E. Moeendarbary, G. Charras, E. Sahai, *Nat. Cell Biol.* **2013**, *15*, 637.
[75] D. Öhlund, E. Elyada, D. Tuveson, *J. Exp. Med.* **2014**, *211*, 1503.
[76] R. Kalluri, *Nat. Rev. Cancer* **2016**, *16*, 582.
[77] R.-P. Czekay, D.-J. Cheon, R. Samarakoon, S. M. Kutz, P. J. Higgins, *Cancers* **2022**, *14*, 1231.
[78] J. M. Houthuijzen, J. Jonkers, *Cancer Metastasis Rev.* **2018**, *37*, 577.
[79] Y. Mezawa, A. Orimo, *FEBS J.* **2022**, *289*, 2429.
[80] L. Rønnov-Jessen, O. Petersen, *Lab Invest* **1993**, *68*, 696.
[81] R. Kalluri, M. Zeisberg, *Nat. Rev. Cancer* **2006**, *6*, 392.
[82] B. C. Özdemir, T. Pentcheva-Hoang, J. L. Carstens, X. Zheng, C.-C. Wu, T. R. Simpson, H. Laklai, H. Sugimoto, C. Kahlert, S. V. Novitskiy, *Cancer Cell* **2014**, *25*, 719.
[83] M. Nurmik, P. Ullmann, F. Rodriguez, S. Haan, E. Letellier, *Int. J. Cancer* **2020**, *146*, 895.
[84] C. Han, T. Liu, R. Yin, *Nonai Roka Seigyo to Baiomaka: Kiban Kenkyu to Shokuhin Sozai* **2020**, *8*, 64.
[85] T. G. Pestell, X. Jiao, M. Kumar, A. R. Peck, M. Prisco, S. Deng, Z. Li, A. Ertel, M. C. Casimiro, X. Ju, *OncoTargets Ther.* **2017**, *8*, 81754.
[86] J. Winkler, A. Abisoye-Ogunniyan, K. J. Metcalf, Z. Werb, *Nat. Commun.* **2020**, *11*, 5120.
[87] Y. Kojima, A. Acar, E. N. Eaton, K. T. Mellody, C. Scheel, I. Ben-Porath, T. T. Onder, Z. C. Wang, A. L. Richardson, R. A. Weinberg, A. Orimo, *Proc. Natl. Acad. Sci. USA* **2010**, *107*, 20009.
[88] J. Liu, S. Chen, W. Wang, B.-F. Ning, F. Chen, W. Shen, J. Ding, W. Chen, W.-F. Xie, X. Zhang, *Cancer Lett* **2016**, *379*, 49.
[89] B. Erdogan, D. J. Webb, *Biochem. Soc. Trans.* **2017**, *45*, 229.
[90] I. Belhabib, S. Zaghdoudi, C. Lac, C. Bousquet, C. Jean, *Cancers* **2021**, *13*, 3466.
[91] F. Ying, M. S. M. Chan, T. K. W. Lee, *Cell Mol Gastroenterol Hepatol* **2023**, *15*, 985.
[92] M. Zhang, F. Zhao, X. Zhang, L. A. Brouwer, J. K. Burgess, M. C. Harmsen, *Mater Today Bio* **2023**, *23*, 100842.
[93] Y. Han, Y. Zhang, T. Jia, Y. Sun, *Tumor Biol.* **2015**, *36*, 1385.
[94] H. Ma, T. Liu, J. Qin, B. Lin, *Electrophoresis* **2010**, *31*, 1599.
[95] A. Nishiguchi, M. Matsusaki, M. R. Kano, H. Nishihara, D. Okano, Y. Asano, H. Shimoda, S. Kishimoto, S. Iwai, M. Akashi, *Biomaterials* **2018**, *179*, 144.
[96] J. Fares, M. Y. Fares, H. H. Khachfe, H. A. Salhab, Y. Fares, *Signal Transduction Targeted Ther.* **2020**, *5*, 28.
[97] A. Forte, B. Rinaldi, L. Sodano, L. Berrino, F. Rossi, M. Finicelli, M. Grossi, G. Cobellis, C. Botti, M. De Feo, *Cardiovasc. Drugs Ther.* **2012**, *26*, 9.
[98] A. Mauretti, A. Neri, O. Kossover, D. Seliktar, P. D. Nardo, S. Melino, *Macromol. Biosci.* **2016**, *16*, 847.